

Self-powered enzyme micropumps

Samudra Sengupta^{1†}, Debabrata Patra^{1†}, Isamar Ortiz-Rivera^{1†}, Arjun Agrawal¹, Sergey Shklyae², Krishna K. Dey¹, Ubaldo Córdova-Figueroa³, Thomas E. Mallouk^{1*} and Ayusman Sen^{1*}

Non-mechanical nano- and microscale pumps that function without the aid of an external power source and provide precise control over the flow rate in response to specific signals are needed for the development of new autonomous nano- and microscale systems. Here we show that surface-immobilized enzymes that are independent of adenosine triphosphate function as self-powered micropumps in the presence of their respective substrates. In the four cases studied (catalase, lipase, urease and glucose oxidase), the flow is driven by a gradient in fluid density generated by the enzymatic reaction. The pumping velocity increases with increasing substrate concentration and reaction rate. These rechargeable pumps can be triggered by the presence of specific analytes, which enables the design of enzyme-based devices that act both as sensor and pump. Finally, we show proof-of-concept enzyme-powered devices that autonomously deliver small molecules and proteins in response to specific chemical stimuli, including the release of insulin in response to glucose.

Self-powered nano- and micropumps that precisely control flow rate in response to external stimuli are critical to the design of the next generation of smart devices. Ideally, the pump should enable fluid flow to be controlled both by the presence and concentration of the specific analyte, such as a substrate, promoter (cofactor) or a related biomarker. This coupling between sensing and transport should allow new applications such as the bottom-up assembly of dynamic structures, cargo delivery at specific locations (for example, drug delivery) and related functions^{1,2}.

Recently, autonomous motion that arises from the catalytic harnessing of chemical free energy from the surrounding environment has been demonstrated at the nano- and microscale^{1–10}. Tethering these catalytic systems to surfaces enables the transfer of the mechanical force to the surrounding fluid. Utilizing this, a variety of pumps have been designed and fabricated that operate on the microscale and function as delivery vehicles for fluids, small molecules and colloids^{11–28}. A major drawback of these artificial micropumps is their non-biocompatibility with respect to the catalyst, fuel or even the ionic-strength regime in which they operate. Biocatalysts, such as enzymes, provide an obvious solution to this problem.

The diffusive mobility of single enzyme molecules has been shown to increase in the presence of a substrate in a concentration-dependent manner and, when exposed to a substrate concentration gradient, ensembles of enzyme molecules exhibit chemotaxis^{29–31}. Enzymes that move by generating a continuous surface force in a fluid should, when fixed in place, function as micropumps that move fluid and colloidal particles in a directed manner. Here we describe a novel enzyme-based platform that combines sensing and microfluidic pumping into a single self-powered microdevice. These micropumps are substrate specific and their pumping speed can be tuned by altering the substrate concentration. In addition, the pumps can be triggered by different analytes that, in situ, generate the substrate for the respective enzymes. This approach demonstrates that even adenosine triphosphate (ATP)-independent enzymes can generate movement and can be used as micropumps in the presence of the appropriate fuel (substrate). Finally, we show that an enzyme-immobilized hydrogel can be used as a scaffold for micropumps that actively pump out gel-entrapped small

molecules and proteins (for example, insulin) in response to a specific chemical trigger (for example, glucose). This opens up the possibility of designing novel stimuli-responsive autonomous cargo and drug-delivery systems³².

Results and discussion

We designed triggered fluid pumps using four different classes of enzymes. Gold (Au) was patterned on a polyethylene glycol (PEG)-coated glass surface. Next, the patterned surface was functionalized with a quaternary ammonium thiol³³, which formed a self-assembled monolayer (SAM) on the Au surface. On incubating the SAM-modified Au surface with enzyme, the negatively charged groups on the enzyme bound selectively to the modified Au surface via electrostatic self-assembly, which resulted in an enzyme pattern on the glass surface (Fig. 1a, Supplementary Fig. 1). To demonstrate the pumping ability of immobilized enzymes, a spacer (20 mm diameter, 1.3 mm height) was placed on top of the enzyme-patterned surface to seal the pump chamber and create a closed system. A buffered solution of substrate with suspended tracer particles was injected into the chamber and the fluid flow was monitored with an optical microscope.

Pumping in the presence of the substrate. We examined catalase³⁴ as our first example of an ATP-independent, enzyme-powered micropump. The enzyme was immobilized selectively on the Au pattern (6 mm diameter) as described above and sulfate-functionalized polystyrene microspheres, 2 μm in size, were used as tracer particles to analyse the fluid flow. In the presence of substrate (hydrogen peroxide) the tracer particles moved towards the Au surface, which indicates that the surrounding fluid is pumped inwards (Supplementary Movie 1). The fluid flow was observed in a closed system, so by fluid continuity the fluid flow showed an outwards motion when viewed above the enzyme-patterned surface. The fluid-pumping velocity showed a substrate concentration and a reaction-rate-dependent increase from 0.37 $\mu\text{m s}^{-1}$ in 0.001 M hydrogen peroxide (enzymatic reaction rate (ν), 12.60 $\mu\text{M s}^{-1}$) to 4.51 $\mu\text{m s}^{-1}$ in 0.1 M hydrogen peroxide (ν , 613.5 $\mu\text{M s}^{-1}$) (Fig. 2a). The Supplementary

¹Department of Chemistry, The Pennsylvania State University, University Park, Pennsylvania 16802, USA, ²Institute of Continuous Media Mechanics, Ural Branch of the Russian Academy of Sciences, Perm 614013, Russia, ³Department of Chemical Engineering, University of Puerto Rico-Mayagüez, Mayagüez, PR 00681, Puerto Rico; [†]These authors contributed equally to this work. *e-mail: asen@psu.edu; tem5@psu.edu

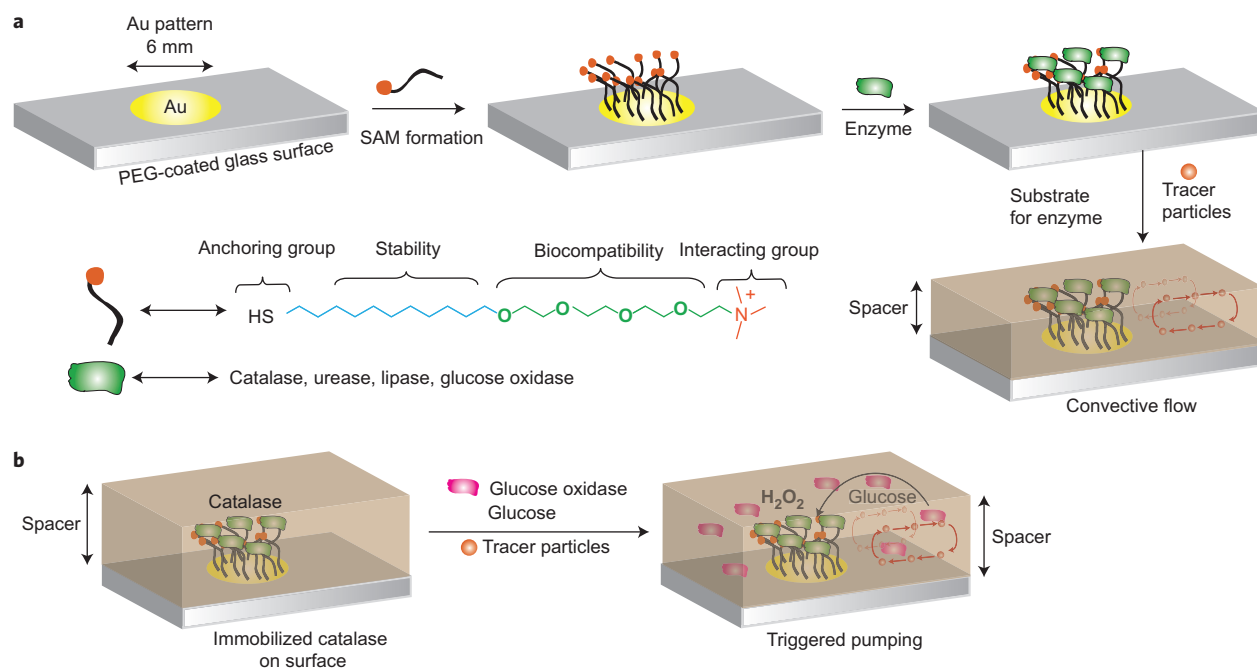


Figure 1 | Schematic that shows the enzyme pattern on a surface and triggered fluid pumping by enzymatic micropumps. a, Au was patterned onto a PEG-coated glass surface using an e-beam evaporator. The patterned surface was functionalized with a quaternary ammonium thiol, which forms a self-assembled monolayer (SAM) on the Au surface. The negatively charged groups on the enzyme bound selectively to the SAM-functionalized Au patterned surface via electrostatic assembly, which resulted in an enzyme pattern on the surface. **b,** Catalase enzyme immobilized on the Au pattern causes fluid pumping triggered by the presence of both GOx and glucose, which generates hydrogen peroxide *in situ*.

Information gives detailed calculations of the reaction rates: the k_{cat} (turnover number) and K_M (substrate concentration at which the reaction rate is half of the maximum rate for the system) values used are for enzymes in solution; these values will be different for immobilized enzymes that are restricted dimensionally. No fluid pumping was observed in the absence of substrate (Supplementary Movie 2). Similar pumping behaviour was also observed for lipase³⁵ and glucose oxidase (GOx)³⁶ in the presence of their respective substrates, 4-nitrophenyl butyrate and glucose, with inwards fluid flow near the Au surface and an outwards flow when viewed above the surface. As with catalase, the pumping velocity increased with increasing substrate concentration and, in turn, enzymatic reaction rates in general (Fig. 2c,d).

The opposite fluid flow was observed for urease anchored to the Au surface. Close to the glass surface, the tracer particles moved away from the Au pattern, which indicates that the surrounding fluid was pumped outwards (Supplementary Movie 3). When viewed upwards in the solution (away from the glass surface), by fluid continuity an inwards fluid flow was observed. As expected, the pumping velocity increased on increasing substrate concentration from $0.24 \mu\text{m s}^{-1}$ in 0.001 M (v , $44.83 \mu\text{M s}^{-1}$) urea to $0.80 \mu\text{m s}^{-1}$ in 0.75 M urea (v , $102.9 \mu\text{M s}^{-1}$) (Fig. 2b). No fluid pumping was observed in the absence of urea.

The newly designed enzyme-powered micropumps clearly have the ability to sense substrate in the surrounding media and initiate fluid pumping in response. Using glucose and GOx, fluid pumping in the catalase pump was triggered by *in situ* generation of hydrogen peroxide (Fig. 1b, Supplementary Movie 4). In the presence of 50 mM glucose and $0.1 \mu\text{M}$ GOx, with catalase immobilized on the Au pattern, the fluid was pumped inwards at a speed of $1.2 \mu\text{m s}^{-1}$. Pumping was not observed in the absence of either glucose or GOx, or both. Thus, in principle, the enzyme pumps can be triggered by a variety of analyte molecules, which opens up the possibility of designing enzyme-based devices that act both as sensor and as pump.

Temporal and spatial variations in pumping. The temporal velocity profile was investigated for all four enzyme-powered pumps over both short and long time intervals. In the case of catalase, fluid pumping was monitored for a duration of ten minutes, at a distance 50–100 μm away from the enzyme pattern and for time intervals of one minute. No significant change in the velocity of tracer particles was observed at each of the three different concentrations of hydrogen peroxide (10 mM, 50 mM and 100 mM) within the time frame of ten minutes (Supplementary Figs 2 and 3). Similar time-dependent studies of pumping speed with urease in 0.75 M urea, GOx in 1 M glucose and lipase in 0.5 M 4-nitrophenyl butyrate showed no appreciable change in pumping velocity at short time intervals (Supplementary Fig. 2). As expected, over longer time scales, the pumping velocity decreased. As the substrate was consumed, the reaction rate decreased and thereby slowed the fluid-pumping speed. This was demonstrated with catalase in the presence of 0.050 M hydrogen peroxide at monitored at regular time intervals of 30 minutes for a duration of four hours (Fig. 3a). Similar behaviour was observed with urease-powered pumps in the presence of 1 M urea (Supplementary Fig. 4). Significantly, these pumps can be recharged by introducing fresh substrate solution after the initial substrate solution is exhausted and fluid pumping stops (Supplementary Fig. 5). For both catalase and urease, fluid pumping resumed with a velocity similar to that observed previously at that specific substrate concentration.

The spatial velocity profile was also examined for each of these enzyme pumps. The fluid-pumping velocity was examined at set distances moving away from the enzyme-functionalized Au pattern. At shorter distances (50–400 μm), the pumping velocities did not show significant variations for catalase-, urease-, GOx- and lipase-powered pumps (Supplementary Fig. 6). As expected, the pumping velocity decreases at longer distances, as observed for catalase- (Fig. 3b) and urease-powered (Supplementary Fig. 4)

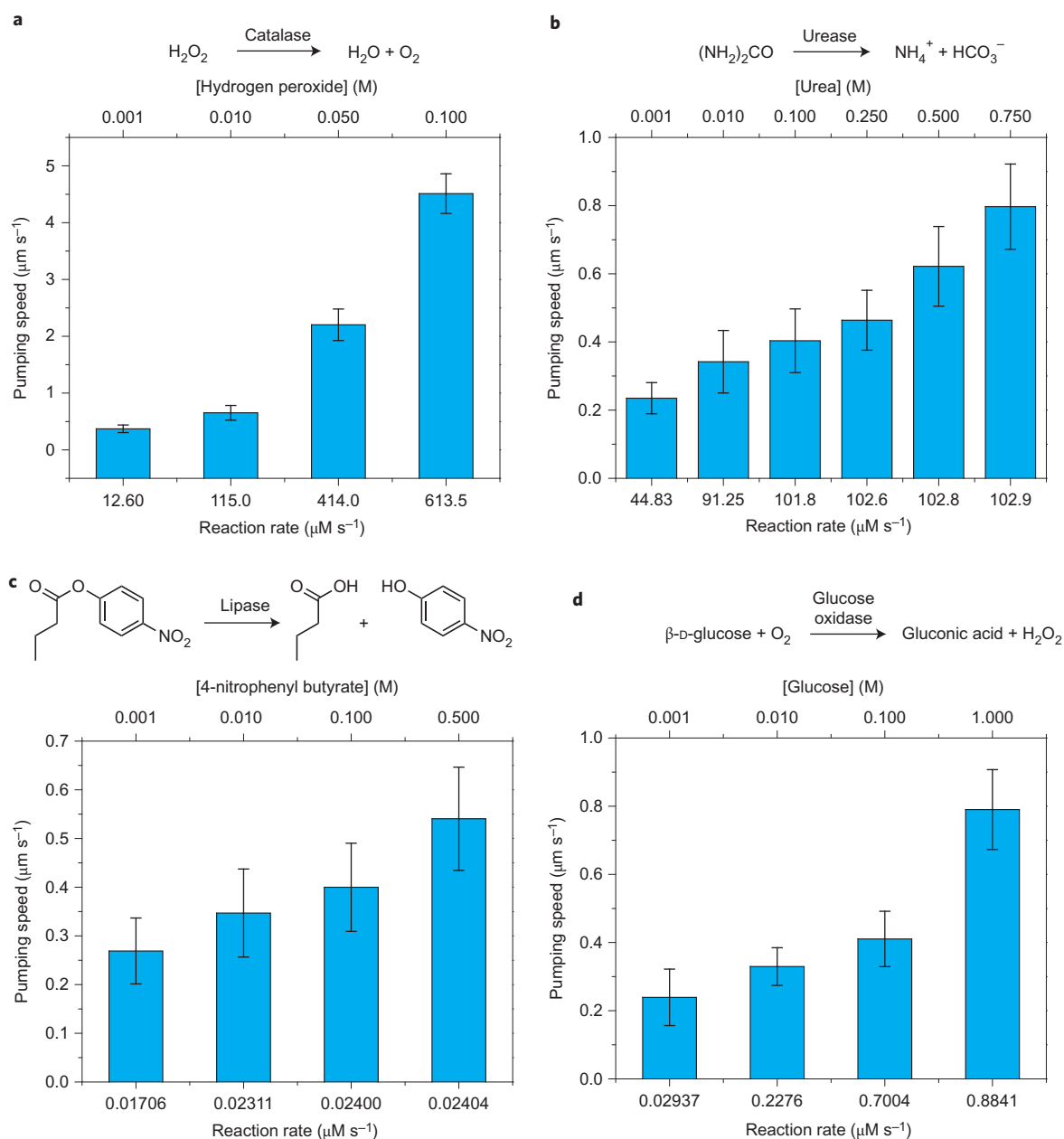


Figure 2 | Fluid pumping velocity in an enzyme-powered micropump as a function of substrate concentration and reaction rate. **a**, Pumping velocity in a catalase-powered micropump increases in the presence of its substrate in a reaction-rate-dependent fashion, at substrate concentrations that ranged from 0.001 M to 0.1 M hydrogen peroxide. **b**, Pumping velocity in a urease-powered micropump increases on increasing the substrate concentration from 0.001 M to 0.75 M urea. **c**, Pumping velocity in a lipase-powered micropump shows a concentration-dependent increase at substrate concentrations from 0.001 M to 0.5 M 4-nitrophenyl butyrate. **d**, Pumping velocity in a GOx-powered micropump increases in a substrate concentration- and reaction-rate-dependent manner from 0.001 M to 1 M glucose. The reaction-rate calculations are based on k_{cat} and K_M values for enzymes in solution. Error bars represent standard deviations. The means and standard deviations are calculated for 30 tracer particles. The pumping velocities at different substrate concentrations are statistically different ($P < 0.01$) (see the Supplementary Information).

pumps monitored at distance intervals of 1,000 μm , for an overall distance of 5,000 μm .

Pumping mechanism. Figure 2 suggests that pumping velocity is generally proportional to the reaction rate, which in turn is controlled by both substrate concentration and inherent catalytic activity. A detailed understanding of the mechanism will allow us to a priori predict the limits of reactive sensing and detection for specific analyte–pump combinations. It is possible to rule out several alternative mechanisms. Pumping that arises from phoretic mechanisms^{37,38}, such as diffusiophoresis³⁹, osmophoresis⁴⁰ and

self-electrophoresis⁴¹, has been demonstrated in the past for surface-anchored catalytic particles^{18–24,27}. Symmetry breaking by anchoring catalysts to solid surfaces can lead to chemical gradients because of the asymmetric production or depletion of solute molecules (charged or uncharged)^{38,42–44}. Directional movement of tracers in the catalase-powered pump can arise from a non-electrolyte diffusiophoretic mechanism because of a gradient caused by the conversion of hydrogen peroxide (two reactant molecules) into water and oxygen (three product molecules)^{45,46}. However, such a mechanism can be ruled out from our observations with an inverted pump set-up. When the

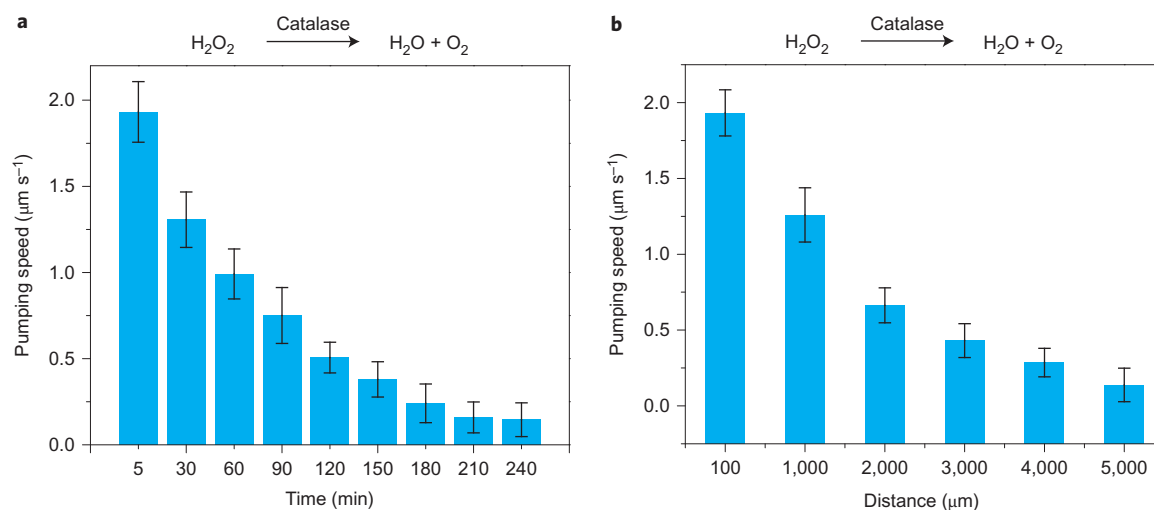


Figure 3 | Temporal and spatial changes in fluid-pumping velocity for catalase-powered micropumps. **a,b**, The fluid-pumping velocity in catalase-powered micropumps in the presence of 50 mM hydrogen peroxide was monitored 50–100 μm away from the enzyme pattern as a function of time at intervals of 30 minutes for a total duration of four hours (**a**), and as a function of distance away from the Au pattern every 1,000 μm for a total distance of 5,000 μm (**b**). As shown, the pumping velocity decreased over time and distance. Error bars represent standard deviations. The means and standard deviations are calculated for 30 tracer particles. The pumping velocities at different time intervals are statistically different from the pumping velocity at time $t = 5$ minutes ($P < 0.01$). The pumping velocities at different distance intervals are statistically different from the pumping velocity at distance $d = 100 \mu\text{m}$ ($P < 0.01$) (see the Supplementary Information).

experimental set-up for the catalase-driven device was turned upside down such that the Au disk was on top, the direction of fluid flow relative to the glass surface reversed (Supplementary Movie 5). Fluid flowed outwards from the Au pattern at the glass surface and, by fluid continuity, moved inwards when viewed away from the surface. If, indeed, a non-electrolyte diffusiophoretic mechanism was in operation, the direction of fluid flow should remain the same irrespective of whether the pump device was upright or inverted.

Transport of fluid in urease-, lipase- and GOx-powered pumps may be the result of an electrolyte diffusiophoretic mechanism because of the generation of charged reaction products^{45,47}. Similar to its non-electrolyte counterpart, electrolyte diffusiophoresis can be ruled out from our observations with inverted pumps. In the case of urease, the direction of fluid flow reversed when the experimental set-up was turned upside down (Au disk on the top). Closer to the surface, the fluid flow was inwards (Supplementary Movie 6), with tracers moving outwards when monitored away from the surface. Further, for both lipase and GOx a similar effect was observed, that is the direction of fluid flow was reversed relative to the pump surface in the inverted set-up. The zeta potential (surface charge) of the tracer particles has a profound effect on the direction of electrolyte diffusiophoretic transport; tracers with opposite charges move in opposite directions. The negatively charged sulfate-functionalized polystyrene tracers moved towards the enzyme-tethered Au pattern for lipase and GOx systems, and moved outwards for urease. If a diffusiophoretic mechanism was in operation, reversing the charge on tracer particles should reverse the direction of their movement. However, when positively charged amine-functionalized polystyrene tracers were used, the direction of their movement remained exactly the same as that of the negative tracers. Moreover, the speed of fluid pumping, monitored with positively charged tracers, was similar to that of their negative counterparts for all the enzyme pumps, which thereby conclusively rules out the possibility of a diffusiophoretic mechanism (Supplementary Fig. 7).

As described above, the direction of fluid flow generated by all four enzyme pumps reversed as the device cavity was inverted. The simplest explanation for this observation is a density-driven mechanism. The enzymatic reactions are exothermic and the

temperature increase at the pump surface should give rise to thermal convection because of the local decrease in fluid density. Thus, in an upright device the flow should be directed upwards from the pump. Fluid continuity means that near the glass surface the flow should be directed towards the Au pattern. For the inverted set-up, the flow direction should be reversed because the lighter fluid tries to occupy the upper layers and spreads along the glass surface away from the Au pattern.

To validate our hypothesis, fluid flow was monitored in the inverted device to determine the pumping velocity. For all four enzyme-powered pumps, the pumping velocities in the inverted set-up were similar to those in the upright one, which strongly suggests a density-driven mechanism as the governing factor (Fig. 4a). Further, the intensity of thermal convective flow within a horizontal layer of liquid in the presence of a temperature gradient is governed by the Rayleigh number (Ra)⁴⁸, such that

$$Ra = \frac{g\beta h^4}{\nu\chi} \frac{dT}{dx} \quad (1)$$

where g , h , β , ν and χ represent the gravitational acceleration, thickness of the liquid layer, volumetric coefficient of thermal expansion, kinematic viscosity and heat diffusivity of the liquid, respectively. The magnitude of the vertical component of the temperature gradient dT/dx can be estimated by calculating the heat flux Q ($\text{J cm}^{-2} \text{s}^{-1}$) as $dT/dx = Q/\kappa$, where κ is the thermal conductivity of the liquid. The heat flux depends on the rate r and enthalpy ΔH of the chemical reaction, as follows:

$$Q = \frac{r\Delta H}{\pi R^2} \quad (2)$$

where R is the radius of the pump surface. Assuming the flow to be steady and small in magnitude, the speed can be scaled as:

$$V \approx \frac{\chi}{h} Ra f(a) \quad (3)$$

where the function $f(a)$ depends on the aspect ratio of the

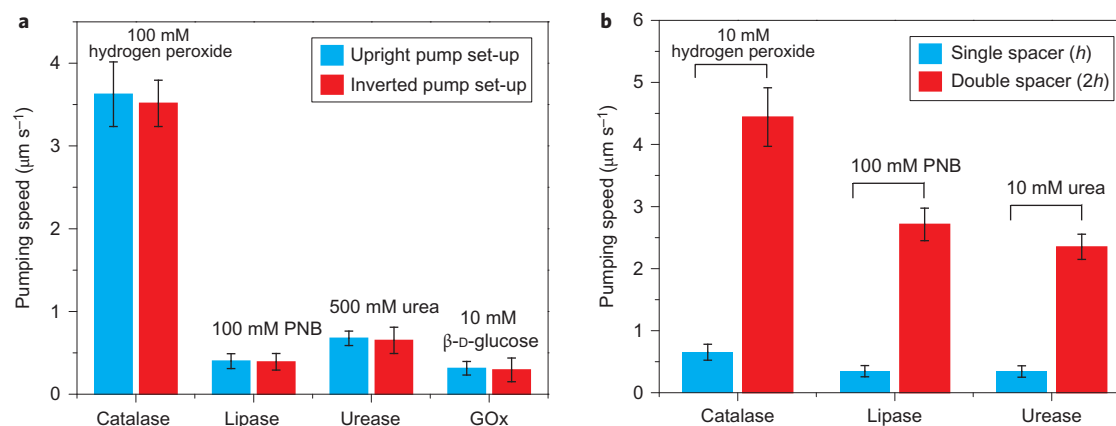


Figure 4 | Fluid pumping in enzyme micropumps generated by density-driven flows. **a**, The fluid-pumping velocity monitored in the upright and inverted pump set-ups showed no significant difference for any of the four enzyme micropumps. Error bars represent standard deviations. The means and standard deviations are calculated for 30 tracer particles. The pumping velocities monitored in the upright and inverted pump set-ups are not statistically different ($P > 0.01$). **b**, The fluid-pumping velocity monitored in the double-spacer (two \times height of chamber, h) set-up showed an approximately seven-fold increase as compared with the single-spacer (h) set-up for three enzyme micropumps. Error bars represent standard deviations. The means and standard deviations are calculated for 30 tracer particles. The pumping velocities monitored in the single- and double-spacer set-ups are statistically different ($P < 0.01$) (see the Supplementary Information).

micropump, $a = R/h$. The flow, therefore, can be characterized by a speed given by:

$$V \sim \frac{g\beta h^3 r \Delta H}{\nu \kappa \pi R^2} f(a) \quad (4)$$

At small Ra the function $f(a)$ can be found by solving two uncoupled boundary-value problems: first, to derive the temperature of the fluid by solving the Laplace equation with the prescribed heat flux at the reactive patch and constant temperature at the upper plate; second, the fluid velocity can be found via the linearized Navier–Stokes–Boussinesq equation. To reiterate, within this linear model, $f(a)$ only changes its sign when the gravity is inverted.

Numerical calculations within this approach showed that $f(a)$ grows from zero up to a value of 10^{-3} , with saturating beyond $R > 3h$. Therefore, for $R > 3h$, any increase in the layer thickness h should result in an increase in the flow speed proportional to h^3 . For smaller a , the prefactor $f(a)$ slightly diminishes this effect. For example, for the experimental set-up with $a = 2.3$ ($R = 3$ mm, $h = 1.3$ mm), the velocity grows by a factor of 6.6 when the layer thickness is doubled. For three different enzymes, the speed increased approximately by a factor of 6.8, which confirms our theoretical proposition (Fig. 4b). Further, assuming that the values of the reaction rate ($r = 10^{-7}$ mol s^{-1}), enthalpy ($\Delta H = 100$ kJ mol^{-1}) and height of the cavity ($h = 1$ mm) are of the same order of magnitude for all the enzymes, the speed was determined as ~ 1 $\mu\text{m s}^{-1}$, in good agreement with the experimental results. Interestingly, even though Ra for our system is fairly high (~ 10), the smaller magnitude of $f(a)$ helps in keeping the flow speed linear in Ra .

In the case of urease, the observed effect is opposite to the expected one. Although the enzyme catalytic reaction is exothermic, the fluid is pumped outwards in the upright device. We hypothesized that as the products of urea hydrolysis are all ionic (NH_4^+ and HCO_3^-), these solvated ions can increase the density of the fluid near the enzyme pattern. This local increase in density causes the fluid to spread along the glass surface, which results in a density-driven convective flow that directs the fluid away from the pattern. In the inverted set-up, the denser fluid generated on the top of the device settles down to lower layers in the cavity, and by fluid continuity

drives the fluid flow inwards near the glass surface. Therefore, in this case the fluid density can be written as:

$$\rho = \rho_0(1 - \beta(T - T_0) + \beta_C(C - C_0)) \quad (5)$$

where ρ is the final fluid density, T is the absolute temperature, C is the concentration of reaction products, ρ_0 , T_0 and C_0 are the reference values of these three characteristics, and β_C is the solute's coefficient of expansion. For $\beta_C > 0$ the fluid density grows as the concentration of products increases. Therefore, for urease the situation is more complicated and double-diffusive convection sets against the competing impacts of the reaction on the flow density and hence on the flow. To verify our hypothesis, the fluid flow was examined in two different systems.

The movement of tracer particles was monitored for the urease pump in a vertical device set-up (Supplementary Fig. 8). The fluid flowed downwards when viewed both below and above the enzyme-patterned surface, which indicates an overall downwards flow at the enzyme-patterned surface in the vertical set-up (Supplementary Movie 7). Again, by fluid continuity the fluid flowed upwards away from the surface. The reaction-generated products, being denser than the reactants, settled to the bottom layers of the device and thereby drove the fluid-flow downwards. The mechanism proposed for the urease-powered micropump can also be established by monitoring the fluid flow using a sink-reservoir model (see Supplementary Information).

Similar experiments that used vertical set-ups were performed with catalase- and lipase-powered micropumps (Supplementary Fig. 8). In both of these cases, the fluid flow was upwards when viewed below the Au pattern close to the surface, against gravity (Supplementary Movie 8). This upwards fluid movement also supports the mechanism proposed previously: convective flows result from a thermal gradient. The increase in temperature at the pump surface caused by these enzyme catalytic reactions decreases the local fluid density for catalase and lipase, and thereby drives the fluid flows upwards. The effect of temperature on solute–particle interaction may also play a role in the observed pumping⁴⁹.

Substrate-triggered release of molecules. The ability of enzyme-powered micropumps to respond to an external stimulus (for example, substrate) and produce a change in the surrounding

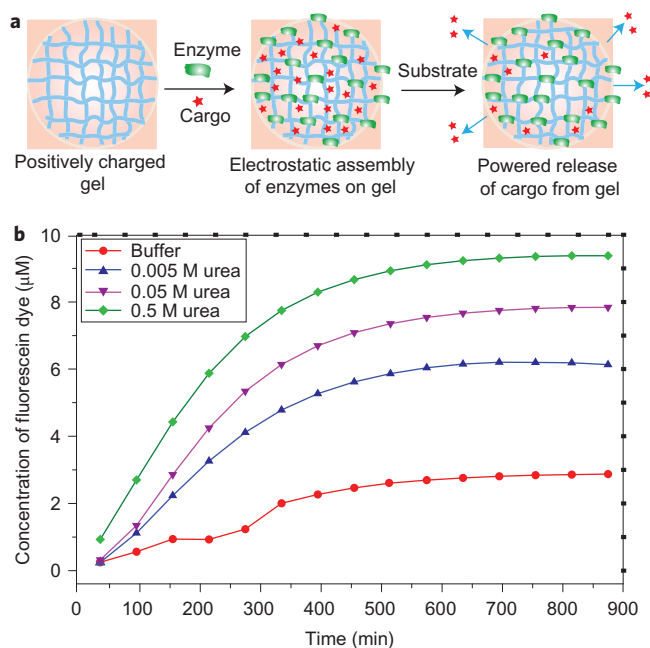


Figure 5 | Urease-powered stimuli-responsive autonomous release of dye.

a, A general schematic that shows the functionalization of enzyme molecules on a positively charged (quaternary-ammonium-terminated) hydrogel, followed by the triggered release of cargo in the presence of the enzyme substrate. **b**, The concentration of dye (fluorescein) molecules (units of μM) released from urease-anchored hydrogel as a function of time in the presence of different concentrations of urea, monitored using a UV-vis spectrophotometer. The profile shows an increase in the amount of dye released from the hydrogel with increasing urea concentration. The concentration of fluorescein dye molecules released was calculated from the absorbance values by using a calibration curve measured for the dye (Supplementary Fig. 9). The initial absorbance measurement was recorded 30 minutes after substrate (urea) addition.

environment by generating fluid flows makes them suitable candidates for applications such as drug delivery, in which a controlled response to an external stimulus is required to attain a specific goal (for example, the triggered administration of a drug). We fabricated a proof-of-concept design to demonstrate the potential ability of the enzyme pumps as autonomous stimuli-responsive drug-delivery devices. Positively charged hydrogels were used as scaffolds for immobilizing enzymes, as well as reservoirs for small molecules. We anticipated the active release of small molecules and proteins from the hydrogel in the presence of the enzyme substrate via a self-pumping mechanism. Hydrogels with quaternary ammonium functionality were synthesized and used as the template for enzyme immobilization via electrostatic self-assembly, similar to the previous pump set-up. As the hydrogel also serves as a reservoir for small molecules (cargo), simultaneous incubation of the hydrogels with enzyme and cargo molecules (to be released) led to their absorption in the gel network. The release of fluorescein dye molecules (used as a model cargo) as a function of time was monitored from the urease-immobilized hydrogel in the presence of varying urea concentrations (Fig. 5) using an ultraviolet-visible (UV-vis) spectrophotometer. Although there was some leaching of dye molecules through passive diffusion in the absence of any substrate, the dye release rate from the hydrogel increased with increasing substrate concentration (Fig. 5b, Supplementary Figs 9–11). This is a direct consequence of fluid pumping regulated by enzymatic reaction. To maintain a stable solution pH, all the measurements were performed in phosphate-buffered

saline (PBS). This ensured that the enzymatic activity was retained and that absorbance analyses were not subject to changes in solution pH, because fluorescein is known to show a pH-dependent change in absorbance.

In another proof-of-concept demonstration, the release of insulin from GOx-immobilized hydrogels was shown at different concentrations of glucose in sodium acetate trihydrate (SAT) buffer (pH 5.23). Increasing levels of insulin release from the hydrogel were achieved with increases in glucose concentration in the surrounding solution (Fig. 6, Supplementary Tables 5–8, Supplementary Figs 12 and 13, and see Supplementary Information for the detailed calculations). The release profile for insulin is somewhat different to that of the dye, presumably because of differences in interaction with the host hydrogel. Our results suggest the design for a rechargeable enzyme pump that can release insulin actively at a rate proportional to the ambient glucose concentration (one of the glucose concentrations employed (0.005 M) is in the physiologically relevant range). The autonomous delivery device described above contrasts with other recently described systems, which involve the passive release of insulin through scaffold decomposition³². Currently, we are exploring our approach with different enzymes and hydrogel systems. We assume that the structural variation of hydrogel is a key parameter for the sustained release of molecules from the cross-linked gel network.

Conclusion

In conclusion, we have demonstrated successfully the first examples of ATP-independent, non-mechanical, self-powered enzyme micropumps. These novel devices were fabricated by simple patterning and electrostatic assembly of enzymes on surfaces. The fluid-pumping speed shows a substrate concentration- and reaction-rate-dependent increase. Catalysis-induced density-driven convective flow is the driving mechanism for the directional fluid pumping. Further, these micropumps can be utilized to attain both spatial and temporal control over fluid transport, as well as delivery of colloids and small molecules. We have also shown that the pumps can be

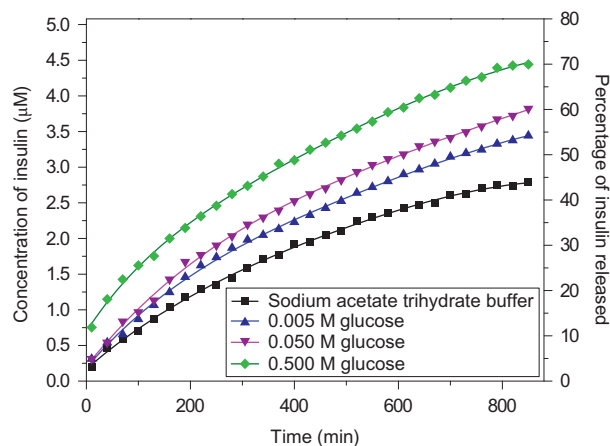


Figure 6 | GOx-powered stimuli-responsive release of insulin. The solution concentration and percentage of insulin molecules released from a GOx-immobilized hydrogel as a function of time in the presence of different concentrations of glucose monitored using a UV-vis spectrophotometer. The profile shows an increase in the amount of insulin released from the hydrogel with increases in glucose concentration in the surrounding solution. The observed behaviour is a direct consequence of the enzymatic reaction-regulated fluid pumping. The concentration of insulin released was calculated using the molar extinction coefficient, $\epsilon_{276} = 6,100 \text{ M}^{-1} \text{ cm}^{-1}$ (Supplementary Information and Supplementary Tables 5–8)⁵⁰. The initial absorbance measurement was recorded ten minutes after substrate (glucose) addition.

triggered by the presence of specific analytes. In principle, the analyte can be a toxic substance that will be drawn towards the pump and be consumed as substrate, and thereby reduce its ambient concentration (for example, a phosphate-based nerve agent as a substrate for a phosphatase pump). Currently, work is in progress to pattern pumps that involve multienzyme cascades to enable regulation and microfluidic logic. Finally, we describe a proof-of-concept device that acts as a self-regulated, stimuli-responsive, active-delivery vehicle.

The ability of immobilized enzymes to pump fluids and particles autonomously with velocities that are dictated by the concentration of a specific analyte, either a second enzyme or a chemical, may enable the development of smart micro- and nanoscale devices that contain sophisticated levels of control over the direction and velocity of fluid and particle transport. From a technological standpoint, this work provides a novel intrinsic energy source for fluid movement that will enhance microfluidic device design and overcome a critical barrier in the field in which pressure-driven pumps are used to move fluids. Further, these self-powered pumps can, in principle, remain viable and be capable of 'turning on' even after prolonged storage.

Methods

Micro pump design, enzyme immobilization and particle tracking. An electronic-beam (e-beam) evaporator was used to produce the Au pattern on a PEG-coated glass surface (MicroSurfaces). The e-beam evaporated a thickness of 90 nm of Au on the PEG-functionalized surface, with a 10 nm adhesion layer of Cr. The radius of the Au pattern was 3 mm. The surface was cleaned thoroughly with isopropanol followed by acetone and dried by flowing nitrogen. Previously synthesized quaternary ammonium thiol was used for SAM formation on the Au surface. The ligand was dissolved in methanol and the surface was incubated in this overnight at room temperature under an inert atmosphere. Later, the surface was washed several times with methanol followed by PBS buffer, and dried under an inert atmosphere. The SAM-modified surface was incubated in an enzyme solution for 4–5 hours. The negatively charged enzymes bound selectively to the thiol-functionalized Au-patterned surface via electrostatic assembly. The enzyme-functionalized surface was thoroughly washed with PBS to remove any unbound enzyme molecules from the PEG-coated glass surface. The enzyme-patterned surface was covered with a secure-seal hybridization chamber (Electron Microscopy Sciences) with dimensions of 20 mm diameter and 1.3 mm height.

To monitor the fluid flow, in all our experiments functionalized polystyrene microspheres (Polysciences Inc.), 2 μm in size, were introduced as tracers suspended in a buffered solution of substrate. Videos were captured using two different optical set-ups. One set-up comprised an upright optical microscope (Olympus BX60M) with a halogen lamp (12 V maximum, 100 W). Excitation light was focused into the sample through a 50 \times objective (LMPlanFLN 50 \times /0.5 BD ∞ /0/FN26.5, Olympus). Emission light was collected by the objective, passed through interference filters and finally detected by a high-sensitivity CCD (charge-coupled device) camera at 30 frames per second. Videos were recorded using this CCD camera attached to the optical microscope. The other system also included an optical set-up, which comprised an inverted microscope (Zeiss Axiovert 200 MAT) with a halogen lamp (12 V maximum, 100 W). Excitation light was focused into the sample through a 20 \times objective (EC Epiplan-NEOFLUAR 50 \times /0.55 HD DIC ∞ /0, Zeiss) or 50 \times objective (LD EC Epiplan-NEOFLUAR 20 \times /0.5 HD DIC 422472-9960, Zeiss). Emission light was collected by the objective, passed through interference filters and finally detected by a high-sensitivity Flea 3 CCD camera (FL3-U3-32S2C-CS, Point Grey), which has a resolution of 2,080 \times 1,552 pixels at 30 frames per second. This camera was attached to the optical microscope and videos were recorded. To measure fluid-pumping velocity in each experiment, 30 tracer particles were tracked for a 25 second time interval using PhysVis software (Kenyon College).

Preparation of enzyme-functionalized hydrogels. For the preparation of enzyme-functionalized, dye-loaded hydrogels, small pieces of hydrogel (2 mm³) were cut and soaked overnight in a mixture of urease (2 mg ml⁻¹, 3 ml) and fluorescein dye (1 ml saturated) solution in PBS. The solution was kept in the refrigerator overnight and allowed to come to room temperature before the experiments were performed.

For the preparation of enzyme-functionalized, insulin-loaded hydrogels, small pieces of hydrogel (2 mm³) were cut and soaked overnight in a mixture of GOx (2 mg ml⁻¹, 3 ml) and insulin (2 mg ml⁻¹, 3 ml) solution in SAT buffer (pH 5.23, adjusted with 0.1 M HCl). The solution was kept at 4 °C overnight, and brought to room temperature before the experiments were performed.

Release of fluorescein dye from enzyme-functionalized hydrogels monitored with UV-vis spectroscopy. Hydrogel pieces were washed 3–4 times with fresh buffer (PBS

or SAT) to remove any excess enzyme and guest molecules. The gel pieces were transferred to a UV-vis cell and buffer or substrate solution (urea or glucose) of varying concentrations was added to promote the release of the cargo. A Beckman DU-800 Spectrophotometer with a six-cell sampler was used for the measurements in kinetics and time mode, with the analytical wavelength set to 488 nm for fluorescein dye (maximum absorbance wavelength of fluorescein in PBS) and 276 nm for insulin⁵⁰ (maximum absorbance wavelength of insulin in SAT). Both experiments were carried out at 25 °C using 250 nm as the background wavelength. Measurements were set to be taken at periods of 30 or 60 minutes for a total duration of ~15 hours. Initial measurements were taken after 15–30 minutes for the dye-release experiment and after 10–15 minutes for the insulin release one. Dye release from the urease-immobilized hydrogels was analysed in 0 M, 0.005 M, 0.05 M and 0.5 M urea solutions in PBS. Insulin release from GOx-immobilized hydrogels was analysed in 0 M, 0.05 M, 0.25 M and 0.5 M glucose solutions in O₂-saturated SAT. Ultraviolet absorbance was plotted as a function of time at each of these concentrations, which gives a direct correlation between substrate concentration and the amount of dye or insulin molecules released from the gel (Supplementary Tables 5–8, and Supplementary Fig. 9).

Syntheses. Detailed information on the synthesis of quaternary ammonium thiol linker, the selective attachment of enzyme molecules to the SAM-modified Au pattern and the synthesis of hydrogel are provided in the Supplementary Information.

Received 8 August 2013; accepted 11 February 2014;
published online 30 March 2014

References

- Sengupta, S., Ibele, M. E. & Sen, A. Fantastic voyage: designing self-powered nanorobots. *Angew. Chem. Int. Ed.* **51**, 8434–8445 (2012).
- Patra, D. *et al.* Intelligent, self-powered, drug delivery systems. *Nanoscale* **5**, 1273–1283 (2013).
- Wang, J. Can man-made nanomachines compete with nature biomotors? *ACS Nano* **3**, 4–9 (2009).
- Sanchez, S. & Pumera, M. Nanorobots: the ultimate wireless self-propelled sensing and actuating devices. *Chem. Asian J.* **4**, 1402–1410 (2009).
- Hong, Y., Velegol, D., Chaturvedi, N. & Sen, A. Biomimetic behavior of synthetic particles: from microscopic randomness to macroscopic control. *Phys. Chem. Chem. Phys.* **12**, 1423–1425 (2010).
- Mei, Y., Solovov, A. A., Sanchez, S. & Schmidt, O. G. Rolled-up nanotech on polymers: from basic perception to self-propelled catalytic microengines. *Chem. Soc. Rev.* **40**, 2109–2119 (2011).
- Mirkovic, T., Zacharia, N. S., Scholes, G. D. & Ozin, G. A. Nanolocotion—catalytic nanomotors and nanorotors. *Small* **6**, 159–167 (2010).
- Paxton, W. F., Sen, A. & Mallouk, T. E. Motility of catalytic nanoparticles through self-generated forces. *Chem. Eur. J.* **11**, 6462–6470 (2005).
- Pumera, M. Nanomaterials meet microfluidics. *Chem. Commun.* **47**, 5671–5680 (2011).
- Mallouk, T. E. & Sen, A. Powering nanorobots. *Sci. Am.* **300**, 72–77 (2009).
- Laser, D. J. & Santiago, J. G. A review of micropumps. *J. Micromech. Microeng.* **14**, R35–R64 (2004).
- Nisar, A., Afzulpurkar, N., Mahaisavariya, B. & Tuantranont, A. MEMS-based micropumps in drug delivery and biomedical applications. *Sens. Actuat. B Chem.* **130**, 917–942 (2008).
- Dash, A. K. & Cudworth II, G. C. Therapeutic applications of implantable drug delivery systems. *J. Pharmacol. Toxicol. Methods* **40**, 1–12 (1998).
- Jakeway, S. C., de Mello, A. J. & Russell, E. L. Miniaturized total analysis systems for biological analysis. *Fresenius J. Anal. Chem.* **366**, 525–539 (2000).
- van der Schoot, B., Jeanneret, S., van den Berg, A. & de Rooij, F. A. A silicon integrated miniature chemical analysis system. *Sens. Actuat. B Chem.* **6**, 57–60 (1992).
- Khandurina, J. *et al.* Integrated system for rapid PCR-based DNA analysis in microfluidic devices. *Anal. Chem.* **72**, 2995–3000 (2000).
- Woolley, A. T. *et al.* Functional integration of PCR amplification and capillary electrophoresis in a microfabricated DNA analysis device. *Anal. Chem.* **68**, 4081–4086 (1996).
- Zhang, H. *et al.* Self-powered microscale pumps based on analyte-initiated depolymerization reactions. *Angew. Chem. Int. Ed.* **51**, 2400–2404 (2012).
- Kline, T. R. *et al.* Catalytic micropumps: microfluidic convective flow and pattern formation. *J. Am. Chem. Soc.* **127**, 17150–17151 (2005).
- Ibele, M. E., Wang, Y., Kline, T. R., Mallouk, T. E. & Sen, A. Hydrazine fuels for bimetallic catalytic microfluidic pumping. *J. Am. Chem. Soc.* **129**, 7762–7763 (2007).
- Jun, I. K. & Hess, H. A. A biomimetic, self-pumping membrane. *Adv. Mater.* **22**, 4823–4825 (2010).
- Hong, Y., Diaz, M., Córdova-Figueroa, U. M. & Sen, A. Light-driven titanium-dioxide-based reversible microfireworks and micromotor/micropump systems. *Adv. Funct. Mater.* **20**, 1568–1576 (2010).
- Paxton, W. F. *et al.* Catalytically induced electrokinetics for motors and micropumps. *J. Am. Chem. Soc.* **128**, 14881–14888 (2006).

24. Solovev, A. A., Sanchez, S., Mei, Y. & Schmidt, O. G. Tunable catalytic tubular micro-pumps operating at low concentrations of hydrogen peroxide. *Phys. Chem. Chem. Phys.* **13**, 10131–10135 (2011).
25. Zhang, L. *et al.* Measurements and modeling of two-phase flow in microchannels with nearly constant heat flux boundary conditions. *J. Microelectromech. Syst.* **11**, 12–19 (2002).
26. Hogg, T. & Freitas, R. A. Chemical power for microscopic robots in capillaries. *Nanomedicine: Nanotech. Biol. Med.* **6**, 298–317 (2010).
27. Yadav, V., Zhang, H., Pavlick, R. A. & Sen, A. Triggered 'on/off' micropumps and colloidal photodiode. *J. Am. Chem. Soc.* **134**, 15688–15691 (2012).
28. Andersson, H., van der Wijngaart, W., Nilsson, P., Enoksson, P. & Stemme, G. A valve-less diffuser micropump for microfluidic analytical systems. *Sens. Actuat. B Chem.* **72**, 259–265 (2001).
29. Sengupta, S. *et al.* Enzyme molecules as nanomotors. *J. Am. Chem. Soc.* **135**, 1406–1414 (2013).
30. Muddana, H. S., Sengupta, S., Mallouk, T. E., Sen, A. & Butler, P. J. Substrate catalysis enhances single-enzyme diffusion. *J. Am. Chem. Soc.* **132**, 2110–2111 (2010).
31. Yu, H., Jo, K., Kounovsky, K. L., de Pablo, J. J. & Schwartz, D. C. Molecular propulsion: chemical sensing and chemotaxis of DNA driven by RNA polymerase. *J. Am. Chem. Soc.* **131**, 5722–5723 (2009).
32. Gu, Z. *et al.* Glucose-responsive microgels integrated with enzyme nanocapsules for closed-loop insulin delivery. *ACS Nano* **7**, 8, 6758–6766 (2013).
33. Miranda, O. R. *et al.* Enzyme-amplified array sensing of proteins in solution and in biofluids. *J. Am. Chem. Soc.* **132**, 5285–5289 (2010).
34. Gaetani, G. *et al.* Predominant role of catalase in the disposal of hydrogen peroxide within human erythrocytes. *Blood* **87**, 1595–1599 (1996).
35. Svendsen, A. Lipase protein engineering. *Biochim. Biophys. Acta* **1543**, 223–228 (2000).
36. Raba, J. & Mottola, H. A. Glucose oxidase as an analytical reagent. *Crit. Rev. Anal. Chem.* **25**, 1–42 (1995).
37. Golestanian, R., Liverpool, T. B. & Ajdari, A. Designing phoretic micro- and nano-swimmers. *New J. Phys.* **9**, 126 (2007).
38. Golestanian, R., Liverpool, T. B. & Ajdari, A. Propulsion of a molecular machine by asymmetric distribution of reaction products. *Phys. Rev. Lett.* **94**, 220801 (2005).
39. Anderson, J. L. & Prieve, D. C. Diffusiophoresis: migration of colloidal particles in gradients of solute concentration. *Separ. Purif. Method* **13**, 67–103 (1984).
40. Pavlick, R. A., Sengupta, S., McFadden, T., Zhang, H. & Sen, A. A polymerization-powered motor. *Angew. Chem. Int. Ed.* **50**, 9374–9377 (2011).
41. Moran, J. L. & Posner, J. D. Electrokinetic locomotion by reaction induced charge auto-electrophoresis. *J. Fluid Mech.* **680**, 31–66 (2011).
42. Howse, J. R. *et al.* Self-motile colloidal particles: from directed propulsion to random walk. *Phys. Rev. Lett.* **99**, 048102 (2007).
43. Córdova-Figueroa, U. M. & Brady, J. F. Osmotic propulsion: the osmotic motor. *Phys. Rev. Lett.* **100**, 158303 (2008).
44. Ke, H., Ye, S., Carroll, R. L. & Showalter, K. Motion analysis of self-propelled Pt–silica particles in hydrogen peroxide solutions. *J. Phys. Chem. A* **114**, 5462–5467 (2010).
45. Anderson, J. L. Colloid transport by interfacial forces. *Ann. Rev. Fluid Mech.* **21**, 61–99 (1989).
46. Anderson, J. L., Lowell, M. E. & Prieve, D. C. Motion of a particle generated by chemical gradients. Part 1. Non-electrolytes. *J. Fluid Mech.* **117**, 107–121 (1982).
47. Prieve, D. C., Anderson, J. L., Ebel, J. L. & Lowell, M. E. Motion of a particle generated by chemical gradients. Part 2. Electrolytes. *J. Fluid Mech.* **148**, 247–269 (1984).
48. Strutt, J. W. On convection currents in a horizontal layer of fluid, when the higher temperature is on the underside. *Phil. Mag.* **32**, 529–546 (1916).
49. Zhao, G. & Pumera, M. Macroscopic self-propelled objects. *Chem. Asian J.* **7**, 1994–2002 (2012).
50. Gammeltoft, S. Receptor binding of biosynthetic human insulin on isolated pig hepatocytes. *Diabetes Care* **4**, 2, 235–237 (1981).

Acknowledgements

We gratefully acknowledge financial support by the Penn State Materials Research Science and Engineering Centers under National Sciences Foundation (NSF) grant DMR-0820404 and, in part, by the Defense Threat Reduction Agency (HDTRA1-13-1-0039). This publication was supported by the Pennsylvania State University Materials Research Institute Nanofabrication Lab and the SNF Cooperative Agreement No. ECS-0335765. This publication is also based on work supported by Award No. RUP1-7078-PE-12 of the US Civilian Research & Development Foundation (CRDF Global) and by the NSF under Cooperative Agreement No. OISE-9531011 (joint grant with the Ural Branch of the Russian Academy of Sciences). I.O.-R. acknowledges a NSF Fellowship (DGE-1255832).

Author contributions

S.S., D.P., T.E.M. and A.S. designed the research. S.S., D.P., I.O.-R. and A.A. performed the research. S.S., D.P. and I.O.-R. contributed new reagents and analytical tools. S.S., I.O.-R., K.K.D., S.Sh., U.C.-F., T.E.M. and A.S. analysed the data. S.S., D.P., I.O.-R. and A.S. wrote the manuscript.

Additional information

Supplementary information is available in the [online version](#) of the paper. Reprints and permissions information is available online at www.nature.com/reprints. Correspondence and requests for materials should be addressed to T.E.M. and A.S.

Competing financial interests

The authors declare no competing financial interests.